THE ASTROPHYSICAL JOURNAL, 554:114–125, 2001 June 10

THE POWER SPECTRUM DEPENDENCE OF DARK MATTER HALO CONCENTRATIONS

VINCENT R. EKE,[1] JULIO F. NAVARRO,[2,3] AND MATTHIAS STEINMETZ[1,4]

Received 2000 December 14; accepted 2001 February 9

ABSTRACT

High-resolution N-body simulations are used to examine the power spectrum dependence of the concentration of galaxy-sized dark matter halos. It is found that dark halo concentrations depend on the amplitude of mass fluctuations as well as on the ratio of power between small and virial mass scales. This finding is consistent with the original results of Navarro, Frenk, and White (NFW) and allows their model to be extended to include power spectra substantially different from cold dark matter (CDM). In particular, the single-parameter model presented here fits the concentration dependence on halo mass for truncated power spectra, such as those expected in the warm dark matter scenario, and predicts a stronger redshift dependence for the concentration of CDM halos than proposed by NFW. The latter conclusion confirms recent suggestions by Bullock and coworkers, although this new modeling differs from theirs in detail. These findings imply that observational limits on the concentration, such as those provided by estimates of the dark matter content within individual galaxies, may be used to constrain the amplitude of mass fluctuations on galactic and subgalactic scales. The constraints on ΛCDM models posed by the dark mass within the solar circle in the Milky Way and by the zero point of the Tully-Fisher relation are revisited, with the result that neither data set is clearly incompatible with the "concordance" ($\Omega_0 = 0.3$, $\Lambda_0 = 0.7$, $\sigma_8 = 0.9$) ΛCDM cosmogony. This conclusion differs from that reached recently by Navarro and Steinmetz, a disagreement that can be traced to inconsistencies in the normalization of the ΛCDM power spectrum used in that work.

Subject headings: cosmology: theory — dark matter — galaxies: formation — galaxies: halos — galaxies: structure

1. INTRODUCTION

Due to their large density, the central regions of dark matter halos, where galaxies form according to the current paradigm of structure formation, hold important astrophysical clues to the nature of dark matter. This is why many studies have attempted to constrain dark matter models on the basis of clues to the dark mass distribution gained from detailed studies of the dynamics of gas and stars in individual galaxies. The most straightforward method compares dark mass distributions derived from rotation curves of disk galaxies with detailed predictions of N-body simulations (Frenk et al. 1988; Flores et al. 1993; Flores & Primack 1994; Moore 1994; Moore et al. 1999b), although similar insight can be gained by inspecting the high-order moments of the stellar velocity distribution in spheroid-dominated systems (Carollo et al. 1995; Rix et al. 1997; Gerhard et al. 1998; Cretton, Rix, & de Zeeuw 2000; Kronawitter et al. 2000).

Despite the simplicity of the rotation curve method and the numerous studies reported in the literature to date (see, e.g., Swaters 1999 for a comprehensive list of references), there is still no broad consensus regarding the detailed distribution of dark matter in disk galaxies, a situation that reflects the difficulties associated with obtaining accurate circular velocities over a large dynamic range in radius as well as with accounting for the contribution of the baryonic component to the rotation curve and for the uncertain response of the dark material to the assembly of the galaxy. For example, while constant density "cores" in the dark mass distribution appeared at first to be necessary to explain the rotation curves of low surface brightness (LSB) dwarf galaxies (Flores & Primack 1994; Moore 1994; McGaugh & de Blok 1998), the persuasiveness of the observational evidence for these cores has recently been called into question by careful reanalysis of the observational data sets (van den Bosch et al. 2000; Swaters, Madore, & Trewhella 2000; van den Bosch & Swaters 2000).

At the same time, there is also considerable uncertainty in theoretical predictions of the dark mass distribution at radii as small as those probed by the rotation curve data. Most workers agree that cold dark matter (CDM) halos have density profiles that diverge near the middle (a result that would be at odds with the alleged cores of LSB dwarfs), but there is still controversy as to the exact asymptotic behavior of the density near $r = 0$. The work of Dubinsky & Carlberg (1991), Warren et al. (1992), and, more recently, Navarro, Frenk, & White (1996, 1997, hereafter NFW) suggested that the central density may diverge as fast as r^{-1}, but subsequent work has argued both for steeper (e.g., $r^{-1.4}$ in Moore et al. 1998) and shallower profiles (e.g., $r^{-0.7}$ in Kravtsov et al. 1998, although it should be noted that the authors have apparently now retracted this result, see Klypin et al. 2001). Each of these models predicts, of course, quite different dark matter contributions to disk galaxy rotation curves, making it difficult to provide a sound interpretation of the observational data.

In other words, even if observations could constrain the dark mass distribution near the middle of disk galaxies, there would still be no consensus on the exact significance of that finding for dark matter models. The reasons for the disagreements in the theoretical predictions are still being investigated, but in all probability they reflect the inherent difficulties associated with simulating accurately and reli-

[1] Steward Observatory, 933 North Cherry Avenue, Tucson, AZ 85721.
[2] Department of Physics and Astronomy, University of Victoria, Victoria, BC V8P 1A1, Canada.
[3] CIAR Scholar and Alfred P. Sloan Fellow.
[4] David and Lucile Packard Fellow and Alfred P. Sloan Fellow.

ably the dynamical behavior within individual galaxies, where the density contrast exceeds 10^6. Particles inhabiting these regions go about their orbits thousands of times during a Hubble time, making numerical results highly vulnerable to insidious systematic artifacts associated with the choice of integrator, time stepping, and gravitational softening. Unfortunately, a full account of the dependence of the innermost density profiles of CDM halos on such numerical parameters is still lacking, but the indication is that it will require extreme care and a concerted numerical effort on massively parallel computers to be able to characterize unequivocally the behavior of the dark matter density profile within the regions probed by rotation curve data.

Given the intrinsic difficulty in providing robust theoretical predictions for the shape of the inner density profiles and the unsettled status of the interpretation of current rotation curve data sets, it is important to identify alternative observational and theoretical comparison criteria that are less sensitive to numerical and observational shortcomings. Navarro & Steinmetz (2000a, 2000b, hereafter NS00a, NS00b) have recently argued that one possible choice is to use the total dark matter content within the main body of individual spiral galaxies.

The typical radii involved are of order ~ 10 kpc for a bright spiral, which corresponds to about 3%–5% of the virial radii. These regions are much less affected by numerical resolution issues than the approximately kiloparsec regions probed by rotation curves. Also, by focusing on the total dark mass within this radius rather than on its detailed radial distribution, both observational and theoretical estimates are presumably more reliable. For example, as discussed by NS00a, there are strict upper limits on the dark mass enclosed within the solar circle in the Milky Way from detailed models of Galactic dynamics (Dehnen & Binney 1998; Gerhard 2000). Such a constraint can be extended to other spiral galaxies by examining the zero point of the Tully-Fisher (TF) relation. Indeed, provided that stellar mass-to-light ratios and exponential scale lengths can be estimated reliably, the TF relation allows for direct estimates of the dark mass within a couple of exponential scale lengths from the middle of the galaxy.

NS00a applied these constraints to a number of halos simulated within the ΛCDM scenario and concluded that the dark mass in ΛCDM halos is too centrally concentrated to be consistent with observations. This result added to an uncomfortably long list of concerns regarding the viability of CDM on the scale of individual galaxies, including the survival of a large number of small-mass halos within the virialized body of a parent halo (the "substructure" problem; see Klypin et al. 1999; Moore et al. 1999a), as well as the evidence for constant density cores in dark halos alluded to above. Taken together, the evidence appeared to warrant a radical revision of one or more of the premises of the CDM paradigm, and there has been no shortage of proposals: self-interacting dark matter (Spergel & Steinhardt 2000), warm dark matter (Hogan & Dalcanton 2000), fluid dark matter (Peebles 2000), fuzzy dark matter (Hu, Barkana, & Gruzinov 2001), etc., all aim to provide a model that behaves like CDM on large scales but with reduced substructure and "concentration" on the scale of individual galactic halos.

If the results of NS00a and NS00b hold and ΛCDM halos are too concentrated to be consistent with observations, then what changes are needed in order to reconcile the predictions of this scenario with observations? Are changes in the overall normalization of the power spectrum necessary, or does the *shape* of the ΛCDM spectrum require modification? Do small-scale cutoffs in the power spectrum (as expected in warm dark matter models) help? Or, in a more general sense, what is the relationship between halo concentration and the power spectrum of initial density fluctuations?

These are the questions addressed here through an extensive suite of N-body simulations. A description of the numerical simulations is given in § 2, including details of the various power spectra chosen for this study. Section 3 contains the main results regarding the concentration of dark matter halos and their dependence on the power spectrum, and § 4 uses these results to revisit the viability of the ΛCDM model regarding the Milky Way and Tully-Fisher constraints. Section 5 summarizes the main conclusions.

2. NUMERICAL METHODS

2.1. *Cosmology and Power Spectra*

All of the simulations described here adopt the same cosmological background model: a flat, cosmological constant–dominated universe with matter density parameter $\Omega_0 = 0.3$, $\Lambda_0 = 0.7$, and Hubble parameter $h = 0.65$.[5] Two different power spectrum shapes have been considered. The first is the standard CDM spectrum, in the form given by Bardeen et al. (1986), which is fully characterized by σ_8, the present linear theory amplitude of mass fluctuations in spheres of radius $8\ h^{-1}$ Mpc, and by the value of the "shape" parameter, Γ (Bardeen et al. 1986; Sugiyama 1995).

The second power spectrum shape aims to mimic a warm dark matter (WDM) power spectrum: it is identical to the CDM spectrum on large scales, but its power is reduced on scales smaller than that of a characteristic free-streaming mass, $P_{\rm WDM}(k) = P_{\rm CDM}(k) \exp\,[-kR_f - (kR_f)^2]$, where R_f is the comoving free-streaming scale. Following Sommer-Larsen & Dolgov (2001) and Avila-Reese et al. (2001), a free-streaming wavenumber, k_f, is defined as that where the WDM power spectrum is half the value for CDM. This implies $k_f \approx 0.46/R_f$. The free-streaming mass is defined as

$$M_f = \frac{4\pi}{3}\,\bar{\rho}_{\rm WDM}\left(\frac{\lambda_f}{2}\right)^3 , \qquad (1)$$

with $\lambda_f = 2\pi/k_f$ and $\bar{\rho}_{\rm WDM}$ being the density of WDM. Expressing the free-streaming mass in terms of the free-streaming scale yields

$$M_f = 3.7 \times 10^{14}\Omega_0 (R_f/h^{-1}\ {\rm Mpc})^3\ h^{-1}\ M_\odot . \qquad (2)$$

This approximation to the actual WDM cosmogony neglects the nonzero velocity dispersion of the warm dark matter particle candidates, but recent work indicates that this omission should have negligible consequences for the quantities of interest here (Avila-Reese et al. 2001; Bode, Ostriker, & Turok 2000). On the other hand, one advantage of this approximation is that the only difference between the CDM and WDM runs is the small-scale behavior of the power spectrum, which implies that systematic trends of halo structure with power spectrum shape are easier to identify.

[5] The present value of the Hubble constant is parameterized by $H_0 = 100\,h\,{\rm km\,s^{-1}Mpc^{-1}}$.

Table 1 contains a list of the specific parameters chosen for the various models, and Figure 1 shows $\sigma(M)$, the $z = 0$ amplitude of linear mass fluctuations in spheres of a given mass corresponding to each power spectrum. In total, seven different models were investigated: five ΛCDM models with different parameter choices for σ_8 and Γ and two WDM models with different free-streaming masses, M_f. Model $S_{0.9}$ will be referred to hereafter as the "fiducial" model, because it is roughly consistent with the local abundance of galaxy clusters (Eke, Cole, & Frenk 1996) and with the amplitude of CMB fluctuations (Stompor, Gorski, & Banday 1995; Liddle et al. 1996). While a value of $\Gamma = 0.2$ was adopted for this default model, it is worth noting that, according to the fit of Sugiyama (1995), $\Gamma = \Omega_0 h \exp[-\Omega_b - (h/0.5)^{1/2}(\Omega_b/\Omega_0)]$, and therefore $\Gamma \approx 0.16$ would be a more appropriate value for the high baryon density parameter, $\Omega_b \approx 0.019\ h^{-2} = 0.045$ (for $h = 0.65$), advocated by Tytler et al. (2000).

2.2. *The Simulations*

For each model listed in Table 1, the AP^{3}M code (Couchman 1991) was used to evolve 128^3 dark matter particles in a 32.5 h^{-1} Mpc cube from $z = 24$ to $z = 0$ using 2000 equal steps in expansion factor. At $z = 0$, four halos with circular velocities between 180 and 230 km s^{-1} (similar to that of the Milky Way) were selected for resimulation from a list of halos identified by the spherical overdensity group–finding algorithm (Lacey & Cole 1994). Unless otherwise specified, halo circular velocities, V_Δ, are measured at the virial radius, r_Δ, the radius of a sphere containing a mean density Δ times the critical value. The parameter Δ depends on Ω and Λ according to (e.g., Eke, Navarro, & Frenk 1998)

$$\Delta(\Omega, \Lambda) = 178\begin{cases}\Omega^{0.30} & \text{if } \Lambda = 0\,, \\ \Omega^{0.45} & \text{if } \Omega + \Lambda = 1\end{cases} \tag{3}$$

and is ≈ 100 at $z = 0$ for the cosmology adopted here. In addition to the circular velocity cuts, a criterion of relative isolation was also enforced, so that halos considered for resimulation were restricted to those without neighbors more massive than $2.7 \times 10^{11}\ h^{-1}\ M_\odot$ within 1.5 h^{-1} Mpc. This selection criterion increases the likelihood that the selected halos are close to equilibrium, simplifying the interpretation of the results. Besides the four "Milky Way" halos selected for each cosmogony, further halos extending to circular velocities of order 100 km s^{-1} were also selected for resimulation in the fiducial $S_{0.9}$ model and the WDM models.

The resimulations were performed using a multiple–time-step N-body code based on the algorithm described by Navarro & White (1993), modified to take advantage of the GRAPE3 hardware (Sugimoto et al. 1990). Particles were allowed to take up to 86,000 time steps during their evolution from the starting redshift of 50 to $z = 0$. Each halo has between 35,000 and 85,000 particles within the virial radius at the final time. A Plummer gravitational softening of $\epsilon = 0.6$ kpc was used in all resimulations of Milky Way halos. The extra resimulated halos with $V_\Delta < 160$ km s^{-1} were run using $\epsilon = 0.4$ kpc. A few simulations were rerun varying the numbers of particles and indicate that this numerical setup is appropriate for making reliable measurements of the total mass within 5–10 kpc.

TABLE 1

POWER SPECTRUM PARAMETER CHOICES

Label	σ_8	Γ	$M_f/(10^{10}\ h^{-1}\ M_\odot)$
$S_{0.9}$	0.9	0.2	...
$S_{1.2}$	1.2	0.2	...
$S_{1.6}$	1.6	0.2	...
$\Gamma_{0.1}$	0.9	0.1	...
$\Gamma_{0.5}$	0.9	0.5	...
W_1	0.9	0.2	1
W_8	0.9	0.2	8

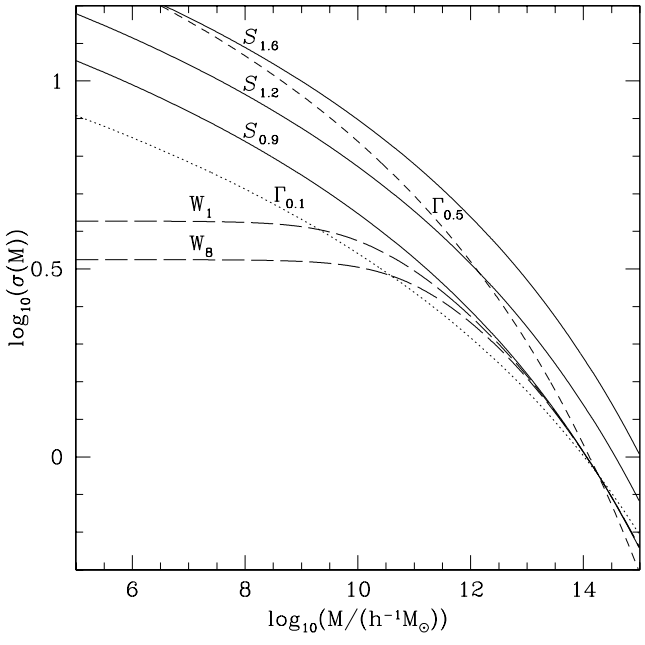

FIG. 1.—The $z = 0$ linear amplitude of mass fluctuations for the seven models investigated in this study. The term $\sigma(M)$ is calculated using a top-hat real-space window function. Solid lines represent, from bottom to top, ΛCDM models $S_{0.9}$, $S_{1.2}$, and $S_{1.6}$. The short-dashed line corresponds to $\Gamma_{0.5}$ and the dotted line to $\Gamma_{0.1}$. The two WDM models are shown with long-dashed lines; the top and bottom lines correspond to models W_1 and W_8, respectively.

3. POWER SPECTRUM AND HALO CONCENTRATION

3.1. *CDM and WDM Density Profiles*

Figure 2 shows the density profiles at $z = 0$ corresponding to the cosmologies listed in Table 1. Each profile is an average over the four Milky Way halos (i.e., halos with V_Δ in the range 180–230 km s^{-1}). The mean profile for each model is shown, together with fits of the form proposed by NFW,

$$\frac{\rho(r)}{\rho_{\rm crit}} = \frac{\delta_c}{(r/r_s)(1 + r/r_s)^2}\,, \tag{4}$$

where $\rho_{\rm crit} = 3H^2/8\pi G$ is the critical density for closure, δ_c is a characteristic density contrast, and r_s is a scale radius that corresponds to the region where the logarithmic slope of the density equals the isothermal value, $d\ln(\rho)/d\ln(r) = -2$.

The main point to note here is that the NFW fitting formula works quite well for ΛCDM halos in the radial range $0.1r_s$–$10r_s$, in agreement with the results of NFW. This fitting formula also reproduces the density profiles of WDM halos, even for mass scales well below the free-

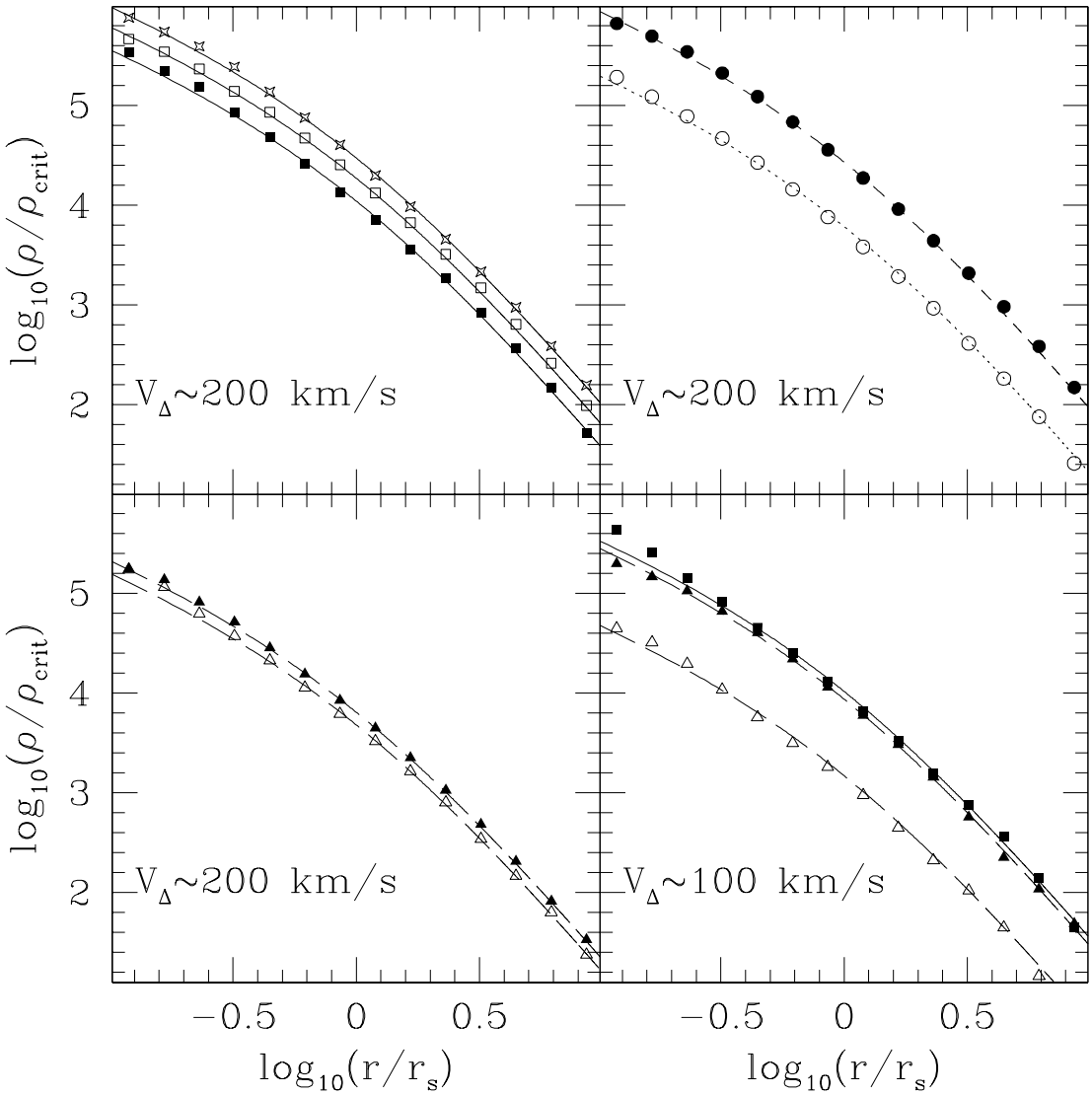

FIG. 2.—Density profiles of dark matter halos formed in the different cosmological models. Different symbols correspond to different models as follows: *filled squares*, $S_{0.9}$; *stars*, $S_{1.6}$; *open squares*, $S_{1.2}$; *open circles*, $\Gamma_{0.1}$; *filled circles*, $\Gamma_{0.5}$; *filled triangles*, W_1; and *open triangles*, W_8. Profiles shown are averages over the four Milky Way halos ($V_\Delta \sim 200$ km s^{-1}) resimulated for each cosmogony. A second average halo is also shown in the lower right panel for models $S_{0.9}$, W_1, and W_8 corresponding to $V_\Delta \sim 100$ km s^{-1}. The curves show NFW profiles fitted to the average profiles. Line types are as in Fig. 1.

streaming mass, M_f. This result has been noted before (Huss, Jain, & Steinmetz 1999; Avila-Reese et al. 2001; Bode et al. 2000) and allows the characterization of each halo by two simple parameters: the mass inside r_Δ (the virial mass M_Δ) and the concentration $c_\Delta = r_\Delta/r_s$. The concentration is directly related to the NFW characteristic density contrast by

$$\delta_c = \frac{\Delta}{3}\frac{c_\Delta^3}{\ln(1+c_\Delta) - c_\Delta/(1+c_\Delta)}, \quad (5)$$

so that either parameter describes fully the density structure of a halo of a given mass. In what follows, c_Δ will be adopted except in the comparison with the results of NFW, where δ_c will be used. This is motivated by the fact that NFW adopted $\Delta = 200$ in their work, whereas the more general Δ definition of equation (3) is adopted here. Note that δ_c is independent of Δ but that concentration is not, so that one should be careful when comparing concentration values quoted by different authors. For the model considered here, $\Delta \approx 100$ at $z = 0$, and $c_\Delta \sim 1.3c_{200}$. Note that although the resolution of these simulations is good enough to measure concentrations in a robust manner, it is not adequate to address the ongoing controversy regarding the innermost slope of the density profile.

3.2. *The Mass Dependence of Halo Concentration*

Figure 3 shows the concentrations measured in the simulations at $z = 0$, as a function of the virial mass of each halo. Different symbols correspond to different cosmogonies, as described in the caption to Figure 2. The top panel corresponds to the three ΛCDM models, $S_{1.6}$, $S_{1.2}$, and $S_{0.9}$, from top to bottom, respectively. The middle panel shows models $\Gamma_{0.5}$ and $\Gamma_{0.1}$, while the bottom panel presents results corresponding to the warm dark matter models W_1 and W_8. Results for the fiducial model $S_{0.9}$ are repeated in all panels.

There are a few things to note in this figure. First, ΛCDM concentrations increase with increasing σ_8 and decrease with increasing mass. These trends are consistent with those reported by NFW on the basis of lower resolution simula-

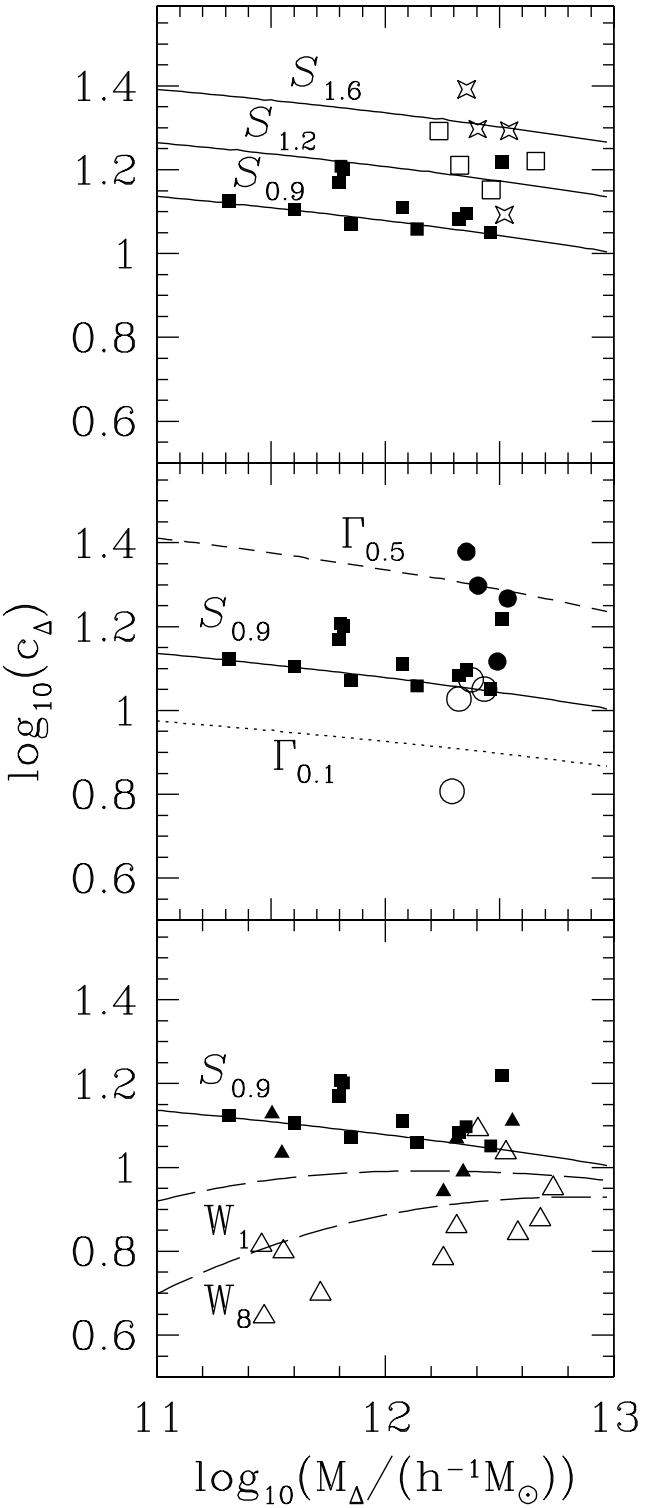

FIG. 3.—Concentration as a function of halo mass for all models, split into three panels for ease of presentation. Lines in each panel are fits to the data using the model described in § 3.3, using the *same* value of $C_\sigma = 28$ (the only free parameter in the modeling) for *all* models. The top panel shows, from top to bottom, ΛCDM models $S_{1.6}$ (*starred symbols*) and $S_{1.2}$ (*open squares*) and the fiducial model $S_{0.9}$ (*filled squares*). The fiducial model is repeated in all panels for comparison. The middle panel shows models $\Gamma_{0.5}$ (*filled circles*) and $\Gamma_{0.1}$ (*open circles*). The bottom panel shows W_1 (*filled triangles*) and W_8 (*open triangles*). All line types are as in Fig. 1.

tions and support NFW's interpretation that the concentration, or equivalently, the characteristic density of a halo, reflects the mean density of the universe at a suitably defined collapse time. Collapse redshifts increase for higher values of the normalization parameter σ_8 and are higher for low-mass systems, reflecting the hierarchical development of structure in CDM universes.

Second, ΛCDM concentrations depend very weakly on mass for the range considered here, changing by only about 50% over two decades in mass for model $S_{0.9}$. Figure 4 shows the simulation results presented by NFW for a variety of different cosmological models and dark matter power spectra, $P(k)$. The weak dependence on mass for the CDM models is surprising when compared with the stronger trends observed for the power-law power spectra simulations, labeled with the spectral index n, where $P(k) \propto k^n$. As n becomes more negative, the concentration depends more weakly upon mass. This is to be expected since, as pointed out by NFW, the scaling between δ_c and M_Δ found in their power-law numerical simulations is $\delta_c \propto M_\Delta^{-(n+3)/2}$, the same that links the characteristic nonlinear mass $M_*(z)$ and the mean cosmic density at redshift z.[6] However, as can be readily seen in Figure 4, the δ_c-M dependence found for CDM models is actually much weaker than expected for $n \sim -1.5$, the "effective" CDM spectral index on the mass scales probed by the NFW simulations. A more negative spectral index seems necessary to explain the CDM results. This led NFW to postulate that it is the amplitude of fluctuations on mass scales *much smaller* than the virial mass that determines the concentration. Consequently, they introduced a (rather arbitrary) parameter of order $\lesssim 1\%$ (see parameter f in equation [7] below) in their modeling, in order to shift the mass scale under consideration and reproduce the numerical results. This is a rather unsatisfactory aspect of their modeling that lacks clear interpretation.

Finally, further clues can be gleaned from the concentration of $\Gamma_{0.5}$ and $\Gamma_{0.1}$ halos. The $\Gamma_{0.1}$ concentrations are lower than $S_{0.9}$, which is not surprising given that the amplitude of mass fluctuations is significantly lower on galactic scales (Fig. 1). On the other hand, $\Gamma_{0.5}$ concentrations are as high as $S_{1.6}$, although $\sigma(M)$ is in this case lower than $S_{1.6}$ on galaxy mass scales (Fig. 1). This again hints that the amplitude on virial mass scales is a poor predictor of the concentration. These hints are confirmed by the results of WDM model W_8, which shows a clear *reversal* of the concentration versus mass trend on scales below a few times the free-streaming mass M_f. The W_8 concentrations *decrease* with decreasing mass despite the fact that WDM $\sigma(M)$ increases toward low masses before saturating at $M \ll M_f$ (Fig. 1).

3.3. *A Model for the Power Spectrum Dependence of the Concentration*

Although the model proposed by NFW captures many of the qualitative trends shown in Figure 3, it suffers from two main shortcomings: (1) it introduces two arbitrary parameters whose interpretation remains unclear and (2) it predicts a redshift dependence for the concentration that is weaker than found in recent numerical simulations (Bullock et al. 2001). Bullock et al. propose an alternative prescription,

[6] The characteristic clustering mass M_* is defined so that $\sigma(M_*)D(z) = \delta_{\rm crit}$ ($=1.686$ for $\Omega = 1$; consult Lacey & Cole 1993 and Eke et al. 1996 for other values of Ω and Λ).

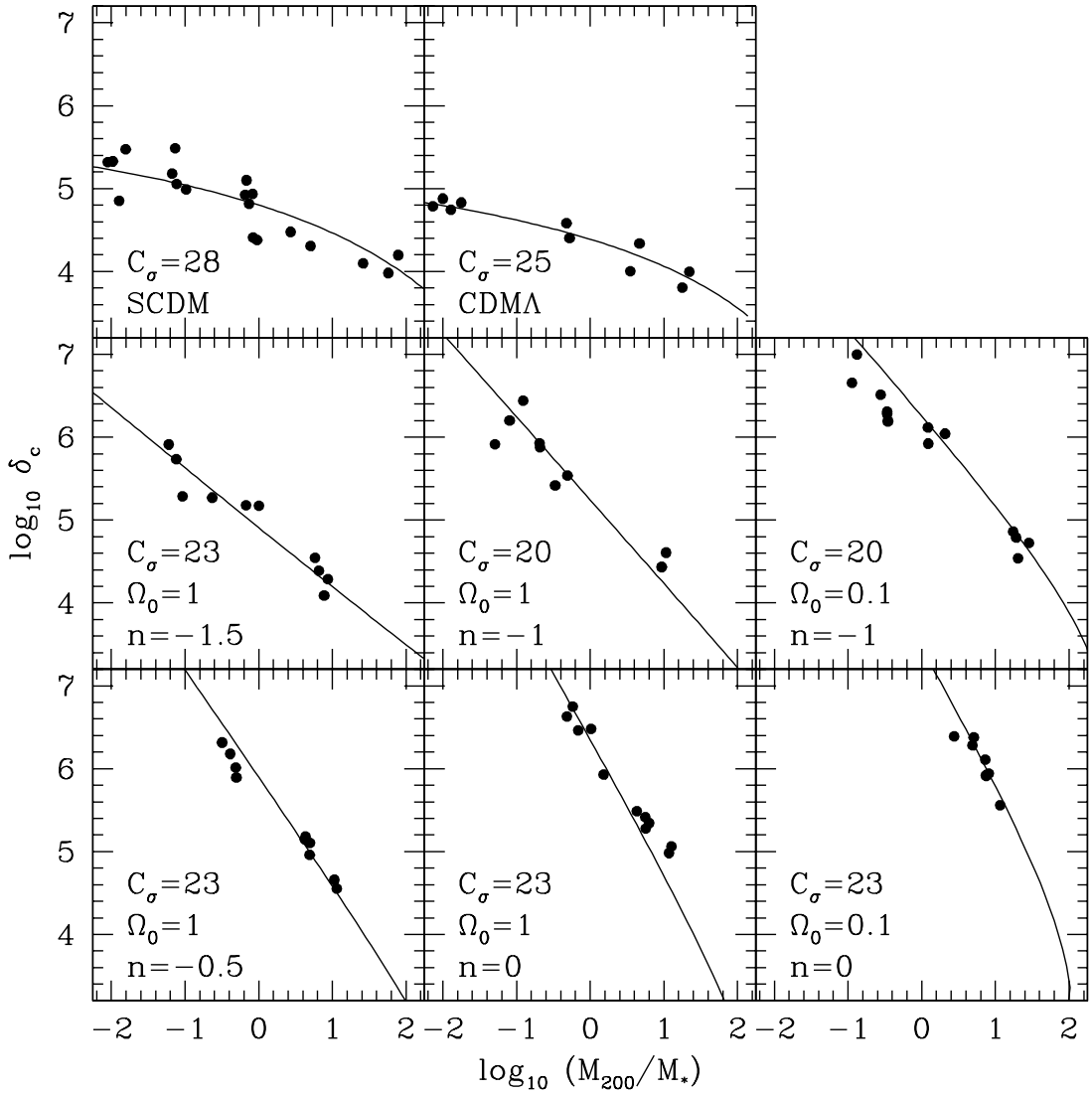

FIG. 4.—Mass dependence of halo characteristic densities, as reported by Navarro et al. (1997; *filled circles*), compared with the results of the model described in § 3.3. Constant C_σ in eq. (13) has been chosen in each case so as to provide a good fit to the simulation results at $M_{200} \approx M_*$. Model SCDM corresponds to the former standard CDM ($\Omega_0 = 1$, $\sigma_8 = 0.63$, $\Gamma = 0.5$). Model CDMΛ has $\Omega_0 = 0.25$, $\Lambda_0 = 0.75$, $\Gamma = 0.19$, and $\sigma_8 = 1.3$. The rest of the panels correspond to power-law power spectra, $P(k) \propto k^n$; the values of n and Ω_0 are listed in each panel. Masses are normalized to the characteristic clustering mass M_*, defined so that $\sigma(M_*) = \delta_{\rm crit}$ ($=1.686$ for $\Omega_0 = 1$). This corresponds to $M_* = 1.6 \times 10^{13}\ h^{-1}\ M_\odot$ for SCDM and $M_* = 4.1 \times 10^{13}\ h^{-1}\ M_\odot$ for CDMΛ. Note that excellent fits can be obtained in all cases with similar values of the single free parameter C_σ.

also with two free parameters, that results in improved agreement between the predicted redshift dependence of concentrations and the results of the numerical simulations. Their model follows NFW in associating a halo's characteristic density with the average background density at collapse time but differs from NFW in the definition of characteristic density and collapse time.

More specifically, NFW take the characteristic density of a halo to be δ_c (see eq. [5]) and use a constant of proportionality, C, to relate this to the mean background density at the collapse redshift, z_c, according to

$$\delta_c = C\Omega(z_0)\left(\frac{1+z_c}{1+z_0}\right)^3 , \tag{6}$$

where z_0 denotes the redshift at which the halo is identified. The collapse time is defined as that when, according to the Press & Schechter approach (Press & Schechter 1974; Lacey & Cole 1993), half the virial mass of the halo was first contained in progenitors more massive than a fraction f of the final mass. This implies that

$$erfc\left\{\frac{\delta_{\rm crit}(z_c) - \delta_{\rm crit}(z_0)}{\sqrt{2[\sigma^2(fM) - \sigma^2(M)]}}\right\} = \frac{1}{2} , \tag{7}$$

where $\delta_{\rm crit}(z) = \delta_{\rm crit}(0)/D(z)$ is the spherical top-hat model linear overdensity threshold and $D(z)$ represents the linear theory growth factor. [The term $D(z) = (1+z)^{-1}$ if $\Omega_0 = 1$, $\Lambda_0 = 0$ is conventionally normalized to unity at $z = 0$; formulae for other values of Ω_0 and Λ_0 can be found in Peebles 1980.] For their simulations, NFW found a good fit by adjusting the two free parameters to be $C = 3000$ and $f = 0.01$.

Bullock et al., on the other hand, choose the characteristic density, $\tilde{\rho}_s$, to be such that

$$M_\Delta = \frac{4\pi}{3} r_s^3 \tilde{\rho}_s \tag{8}$$

and specify the collapse redshift, z_c, solely in terms of $\sigma(M)$, so that

$$D(z_c)\sigma(FM_\Delta) = 1.686\,, \tag{9}$$

where $F = 0.01$. Their second free parameter, K, relates the characteristic density to the background density via

$$\tilde{\rho}_s = K^3\Delta(z_0)\rho_{\rm crit}(z_c) \tag{10}$$

and feeds through into the concentration as

$$c_\Delta = K\left(\frac{1+z_c}{1+z_0}\right). \tag{11}$$

The term $K = 4$ provides a good fit to their ΛCDM simulation results.

This model, like that of NFW, suffers from the introduction of two arbitrary parameters (F and K) whose interpretation remains unclear. Furthermore, the definition of collapse epoch given in equation (9) implies that for a truncated power spectrum such as WDM, halo concentrations will still increase monotonically with decreasing mass, approaching a constant at $M \ll M_f$. This is at odds with the results presented in the previous section (see also Bode et al. 2000), which show that WDM halo concentrations *decrease* on mass scales below a few times the free-streaming mass. These results strongly suggest that it is not only the amplitude of the power spectrum but also its shape that determine the concentration of dark matter halos. In particular, only a modeling that includes such shape dependence will be able to reproduce the somewhat counterintuitive dependence of concentration on halo mass found for truncated power spectra such as W_8 (see Fig. 3).

After some experimentation, a simple model has been produced that matches the mass dependence of halo concentrations for the simulations presented here. Furthermore, the same model also fits all of the original NFW results whilst modifying the redshift dependence of concentrations so that they are compatible with the recent results of Bullock et al. The new model has *a single free parameter* and is of more general applicability, since it can be applied to truncated power spectra, where Bullock et al.'s prescription fails. This model also removes the need for the arbitrary, small mass fraction constant introduced by NFW and Bullock et al. ($f = 0.01$ in eq. [7] and $F = 0.01$ in eq. [9]) by postulating that the concentration of a halo is controlled by a combination of the amplitude *and* shape of the power spectrum.

Consider the effective amplitude of the power spectrum on scale M, defined by

$$\sigma_{\rm eff}(M) = \sigma(M)\left[-\frac{d\ln(\sigma)}{d\ln(M)}(M)\right]. \tag{12}$$

This effective amplitude modulates $\sigma(M)$ so that, for WDM-like spectra, it *decreases* on mass scales smaller than a few times the free-streaming mass M_f. In broad terms, a given mass scale M collapses when $D(z)\sigma(M)$ is at least unity. This time is controlled by the redshift evolution of the linear growth factor, $D(z)$, appropriate for the cosmological model under consideration. Following this, the collapse redshift, z_c, of a halo of mass M may be identified as

$$D(z_c)\sigma_{\rm eff}(M_s) = \frac{1}{C_\sigma}\,, \tag{13}$$

where C_σ is a constant and M_s is the mass contained within $r_{\rm max} = 2.17r_s$, the radius at which the circular velocity of an NFW halo reaches its maximum. The requirement that $D(z_c)\sigma(M_s) \geq 1$ implies that $C_\sigma \geq -(d\ln\sigma/d\ln M)^{-1}$. For a power-law fluctuation spectrum with $P(k) \propto k^n$, then, this yields $C_\sigma \geq 6/(n+3)$. As in the models of NFW and Bullock et al., the mean density of the universe at the collapse redshift can then be used to calculate a characteristic density for the halo. Defining the characteristic density of the halo to be, as in Bullock et al. (see eq. [8]),

$$\tilde{\rho}_s = \Delta(z_0)\rho_{\rm crit}(z_0)c_\Delta^3 \tag{14}$$

and setting this to equal the spherical collapse top-hat density at the collapse epoch, $\rho_{\rm sc}$, where

$$\rho_{\rm sc}(z_c) = \Delta(z_c)\rho_{\rm crit}(z_c) = \Delta(z_c)\,\frac{\bar{\rho}_0(1+z_c)^3}{\Omega(z_c)}\,, \tag{15}$$

yields

$$c_\Delta^3 = \frac{\Delta(z_c)}{\Delta(z_0)}\,\frac{\Omega(z_0)}{\Omega(z_c)}\left(\frac{1+z_c}{1+z_0}\right)^3. \tag{16}$$

Equations (13) and (16) describe the concentration of a halo of given mass, once the single free parameter in eq. (13), C_σ, has been specified. Since the characteristic mass scale at which the effective amplitude of the power spectrum is evaluated depends on r_s and, therefore, on c_Δ, equations (13) and (16) need to be solved iteratively to yield the combination of c_Δ and z_c.[7]

This model reproduces, with roughly the same value of C_σ, the results of the simulations presented here, all of the original results of NFW, as well as the redshift dependence advocated by Bullock et al. This is shown by the curves in Figure 3, which show the result of applying the model, at $z = 0$, to the seven cosmogonies adopted in this study. Solid lines are used for the S models, short-dashed and dotted lines for $\Gamma_{0.5}$ and $\Gamma_{0.1}$, respectively, while long-dashed lines are used for WDM. All of the curves use the same value for the proportionality constant in equation (13), $C_\sigma = 28$. The model reproduces very well the trends with mass, normalization, and shape of the power spectrum seen here, including the counterintuitive trend toward lower concentrations seen in the low-mass W_8 halos. Table 2 contains a list of concentrations for a $10^{12}\,h^{-1}\,M_\odot$ halo identified at $z = 0$ in a variety of commonly studied cosmological models. This illustrates the interplay between Ω_0, Λ_0, σ_8, and Γ.

TABLE 2

VALUES OF c_Δ AND c_{200} FOR A $10^{12}\,h^{-1}\,M_\odot$ HALO IDENTIFIED AT $z = 0$ IN FOUR COMMONLY STUDIED COSMOLOGICAL MODELS

Ω_0	Λ_0	h	σ_8	Γ	c_Δ	c_{200}
1.....	0	0.5	0.5	0.5	12.3	11.7
1.....	0	0.5	0.5	0.2	6.7	6.4
0.3.....	0	0.65	0.9	0.2	18.6	15.2
0.3.....	0.7	0.65	0.9	0.2	12.0	8.9

The model described above also reproduces the original results of NFW quite well. This is shown in Figure 4, where the density contrast δ_c is plotted as a function of the mass enclosed within a $\Delta = 200$ sphere, the parameters used by

[7] An algorithm to perform this calculation for CDM and WDM power spectra is available on request from the authors.

NFW. It is apparent from this figure that the model also reproduces the results of the eight cosmogonies studied by NFW, including open models with Ω_0 as low as 0.1, again with approximately a single value of the constant C_σ.

3.4. *The Redshift Dependence of Halo Concentration*

According to equations (13) and (16), the model predicts that, at fixed halo mass, in an Einstein–de Sitter cosmogony $c_\Delta(M, z)\sigma_{\rm eff}(M_s) \propto (1 + z)^{-1}$. Ignoring the weak dependence of $\sigma_{\rm eff}(M_s)$ upon concentration, this relation agrees with the prediction of the model by Bullock et al. for the evolution of halo concentration. However, for low-density universes the scaling of the linear growth factor $D(z)$ with redshift leads to a greater difference between these models, and it is therefore important to verify that this model is still in good agreement with the numerical results.

Figure 5 compares the predictions of all three different concentration models with the results of the numerical

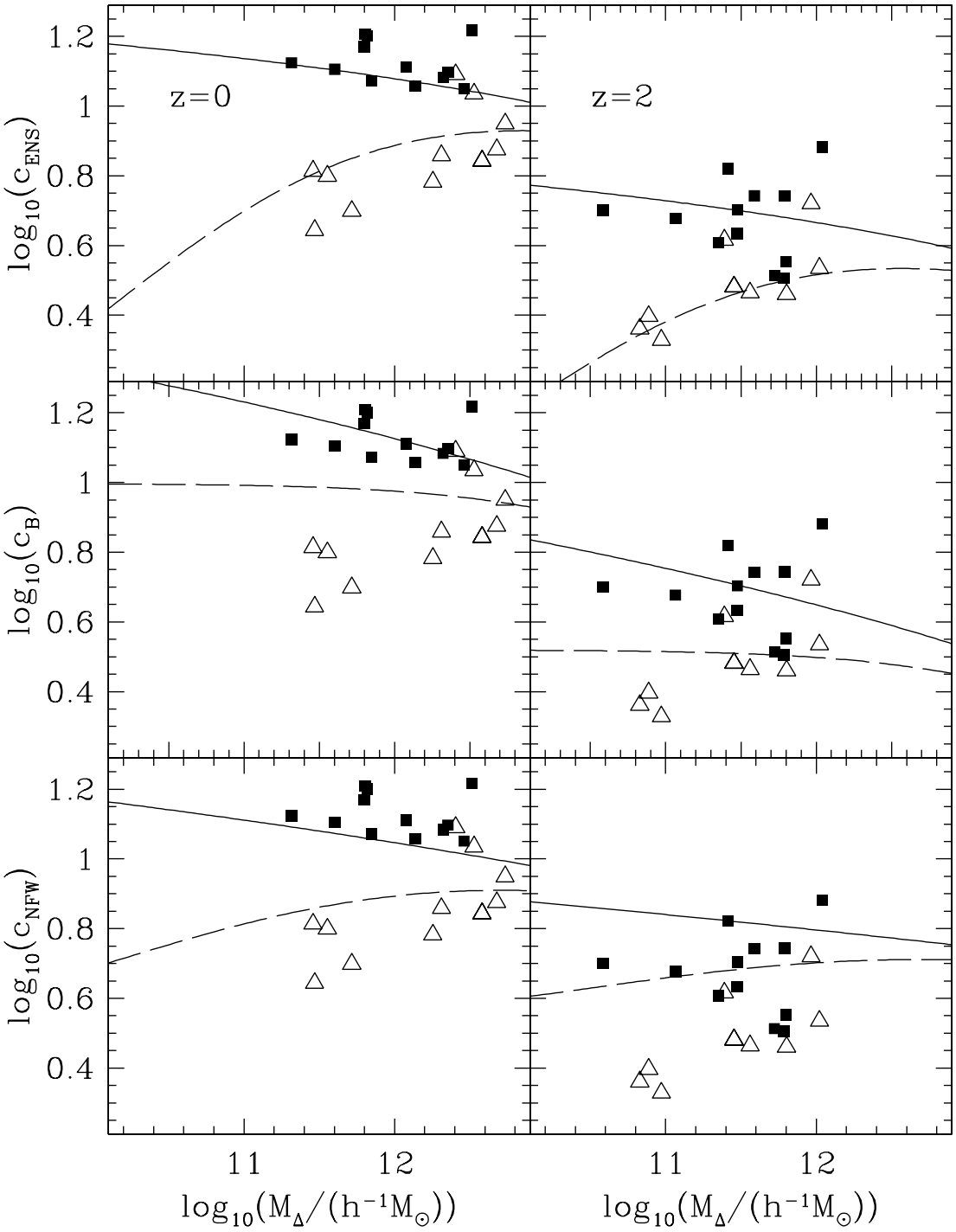

FIG. 5.—Comparison between concentrations measured at $z = 0$ (*left panels*) and $z = 2$ (*right panels*) and the predictions of three different models. ENS corresponds to the model presented in this paper (*top panels*), B to that in Bullock et al. (2001; *middle panels*), and NFW to concentrations computed using the procedure outlined in the Appendix of NFW (*bottom panels*). The filled squares correspond to $S_{0.9}$ halos, whereas open triangles correspond to W_8 halos. The solid and dashed curves show the model predictions for $S_{0.9}$ and W_8, respectively.

simulations at $z = 0$ and 2. The comparison includes all halos in the $S_{0.9}$ and W_8 simulations with more than 2500 particles within r_Δ. Concentrations labeled with an "ENS" subscript in the top row correspond to the model presented here, "B" to Bullock et al.'s (*middle row*), and "NFW" to the NFW model predictions in the bottom panels. ENS concentrations use $C_\sigma = 28$ in equation (13), B concentrations use $F = 0.01$ and $K = 4$, and NFW concentrations use $C = 3000$ and $f = 0.01$. The typical halo mass range probed varies from 10^{11}–$10^{13}\ h^{-1}\ M_\odot$ at $z = 0$ to $10^{10.5}$–$10^{12}\ h^{-1}\ M_\odot$ at $z = 2$.

The top two panels show that the model presented here predicts a redshift dependence in good agreement with the simulation results, both for $S_{0.9}$ and W_8. The middle panels show that the Bullock et al. model also fits the results of the fiducial ΛCDM runs at $z = 0$ and $z = 2$, but that their model fails to capture the mass dependence seen in the W_8 simulations. This illustrates the point that was made earlier that it is the effective normalization (eq. [12]) rather than simply $\sigma(M)$ that determines halo concentrations. The bottom row highlights the weak redshift dependence predicted by the NFW model compared with the simulation results, as noted by Bullock et al.: it slightly underpredicts the fiducial model concentrations at $z = 0$ but overpredicts them at $z = 2$.

In summary, the data in Figure 5 show that the redshift evolution predicted by the model presented here is consistent with the simulation results. Even at $z = 5$, the highest redshift with simulation data in Figure 11 of Bullock et al., the concentrations of $10^{12}\ h^{-1}\ M_\odot$ halos are $c_\Delta = 2.6$ and 2.5 for the model in § 3.3 and that of Bullock et al., respectively. Thus, it is not possible to discriminate between the slightly different redshift dependences of these two models.

4. COMPARISON WITH OBSERVATIONS

4.1. *ΛCDM and the Dark Mass within the Solar Circle*

Observations of star and gas kinematics provide well-defined constraints on the dark matter content of the Milky Way within the solar circle, $R_0 = 8.5$ kpc. As discussed by NS00a (see that paper for full references), a simple upper limit on the dark mass within R_0, $M_{\rm dark}(r < R_0)$, may be obtained by combining the observed circular velocity at the Sun's location, $V_c(R_0) = 220$ km s^{-1}, with estimates for the total mass and exponential scale length of the Galactic disk ($M_{\rm disk} = 6 \times 10^{10}\ M_\odot$ and $r_{\rm disk} = 3.5$ kpc, respectively). The result (note that there is a typo in eq. [1] of NS00a),

$$M_{\rm dark}(r < R_0) \lesssim 4.3 \times 10^{10}\ M_\odot\ , \qquad (17)$$

constitutes an upper limit because the simple calculation described above neglects two potentially important effects: (1) the contribution of the bulge and (2) any potential contraction that the dark halo may have experienced as a result of the assembly of the galaxy.

The constraint expressed in equation (17) is straightforward to compare with the results of the numerical simulations described here. This is done in Figure 6, where the dark mass within 8.5 kpc is plotted as a function of V_{200}, the halo circular velocity for $\Delta = 200$ used in NS00a, for all of the halos. The top panel shows halos formed in the $S_{0.9}$, $S_{1.2}$, and $S_{1.6}$ models, the three different normalizations chosen for the ΛCDM scenario. At $V_{200} = 220$ km s^{-1} (marked with an arrow in Figure 6), $M_{\rm dark}(r < R_0)$ increases approximately in proportion to σ_8. In light of the modeling

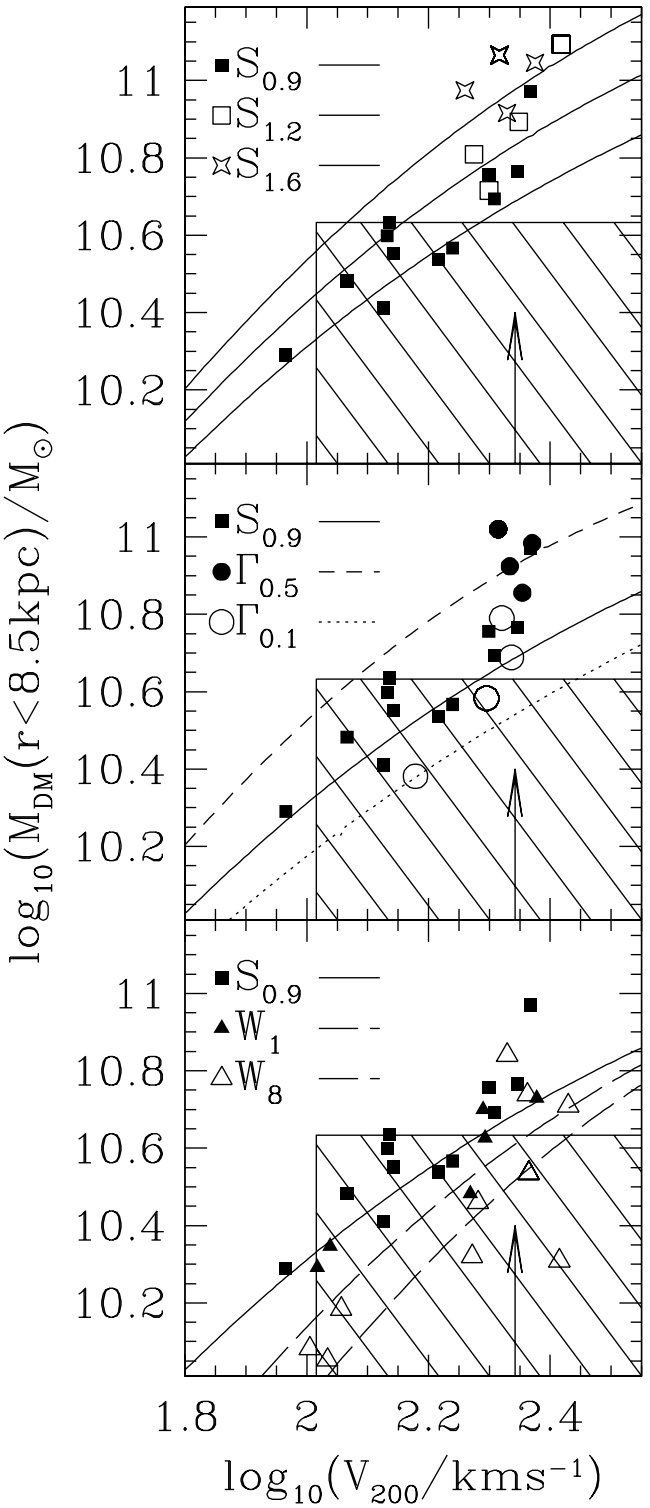

FIG. 6.—Dark matter halo masses within the solar circle (8.5 kpc) compared with constraints derived from dynamical observations of the Milky Way (*hatched region*). A vertical arrow marks a circular velocity of 220 km s^{-1}. The different symbols correspond to different cosmogonies, as specified in Fig. 2. Lines correspond to NFW profiles assuming concentrations given by the model in § 3.3.

described above, this can be attributed to the higher average collapse times that result from the choice of higher normalizations.

The lines in this panel correspond to the mass within 8.5 kpc predicted by the model described in § 3.3. Combining

this model with the constraint in equation (17), it is possible to estimate the range of circular velocities allowed for the halo of the Milky Way as a function of the normalization parameter σ_8:

$$\sigma_8 v_{220} m_{\rm dark} < 0.8 , \quad (18)$$

where v_{220} is the circular velocity, V_{200}, of the Milky Way halo in units of 220 km s^{-1} and $m_{\rm dark}$ is $M_{\rm dark}/(4.3 \times 10^{10} M_\odot)$. This suggests that, for $\Gamma = 0.2$, the circular velocity of the halo of the Milky Way should be somewhat less than 220 km s^{-1}, unless $\sigma_8 < 0.9$ or the Milky Way halo has an unusually low concentration for its mass. The fiducial $S_{0.9}$ model may be reconciled with the Milky Way constraint if $V_{200} \lesssim 195$ km s^{-1}. A knock-on effect of moving the Milky Way into a smaller halo would be that any predictions of the galaxy luminosity function made by mapping mass into luminosity using the properties of the Milky Way would find that Milky Way–type galaxies were more abundant than before. As $M \propto V^3$ and assuming that the luminosity of a galaxy is proportional to its mass, it only takes a 20% decrease in halo circular velocity to halve the luminosity. Thus, it remains to be seen whether assigning the luminosity of the Milky Way to the many halos with $V_{200} \approx 195$ km s^{-1} is consistent with the luminosity function of bright spirals (see, e.g., Cole et al. 1994, 2000).

A lower bound on the mass of the Milky Way halo may be derived by requiring that the total baryonic mass of the Galaxy does not exceed the baryon mass within the virial radius of the halo. Assuming $\Omega_b = 0.019\ h^{-2} \approx 0.045$, the minimum halo mass corresponds to a circular velocity of ~ 105 km s^{-1}. This is lower than the 130 km s^{-1} derived by NS00a, because of the lower baryon fraction ($\Omega_b = 0.0125\ h^{-2}$) and slightly higher Hubble constant ($h = 0.7$) adopted by those authors.

From Figure 6, halos in the fiducial $S_{0.9}$ ΛCDM model with circular velocities in the range 105–190 km s^{-1} appear consistent with the Milky Way constraint. For $\sigma_8 = 1.2$, the range of acceptable halo masses is narrower, and essentially no halo agrees with the observational constraints if $\sigma_8 = 1.6$. This is reminiscent, although less stringent, of the conclusion reached by NS00a, who argued that $\sigma_8 = 1.14$ ΛCDM halos were too concentrated to be consistent with this constraint. However, a reanalysis of the NS00a data set reveals that because of inconsistencies in the normalization procedure for their ΛCDM simulations,[8] those authors had effectively normalized their power spectra to $\sigma_8 \sim 1.6$ rather than $\sigma_8 = 1.14$. After correcting for this error, the results in NS00a and NS00b are consistent with those reported here.

4.2. *The Zero Point of the Tully-Fisher Relation*

As discussed by NS00a and NS00b, the analysis of § 4.1 can be extended to other spiral galaxies by examining the correlation between galaxy luminosity and the rotation speed of their gas and stars: the Tully-Fisher relation (Tully & Fisher 1977). Provided that stellar mass-to-light ratios and exponential scale lengths can be estimated reliably, it is possible to evaluate the disk contribution to the circular velocity at 2.2 exponential scale lengths (where the disk contribution peaks and optical Tully-Fisher velocities are typically measured) and derive constraints on the total dark mass contained within this radius.

The more concentrated a halo is, the faster a disk of given mass and radial scale must rotate to attain centrifugal equilibrium. Thus, as shown by NS00a and NS00b, the zero point of the Tully-Fisher relation provides a direct constraint on halo concentrations. Although these authors conclude that $\sigma_8 = 1.14$ ΛCDM halos are too concentrated to be consistent with the I-band Tully-Fisher relation, as discussed in § 4.1 their conclusions were affected by an inconsistent normalization of the power spectrum. Given that the simulations of NS00a and NS00b effectively probed a $\sigma_8 \approx 1.6$ ΛCDM model and concentration depends strongly on σ_8, it is appropriate to revisit the issue and verify whether the fiducial $S_{0.9}$ model is consistent with observations.

4.2.1. *Gasdynamical Simulations*

To this aim, a number of gasdynamical simulations including star formation and feedback have been run using GRAPESPH, a code that combines the hardware N-body integrator GRAPE with the smoothed particle hydrodynamics (SPH) technique (Steinmetz 1996). The simulation setup and analysis are identical to those described in Navarro & Steinmetz (1997) and Steinmetz & Navarro (1999), and the reader is referred there for details. In brief, the same initial conditions described above for the dark matter–only runs are used with the addition of gas, assuming a value of $\Omega_b = 0.0125\ h^{-2}$ for the baryon density parameter. Models with gas have typically 20,000 gas particles and the same number of dark matter particles. Up to 5000 of these end up in a galaxy at $z = 0$, resulting in lower resolution than the N-body simulations discussed in previous sections. Gas particle masses range from 4.5×10^6 to $2.5 \times 10^8\ M_\odot$, depending on the model considered.

Model galaxies are unmistakably identified in the runs as star and gas clumps with high density contrast. Only halos with more than 500 dark particles within the virial radius have been retained for analysis. The properties of the luminous component are computed using the star particles within a radius, $r_{\rm gal} = 20(V_{200}/220\ {\rm km\ s^{-1}})\ h^{-1}$ kpc, and assuming either a Scalo or Salpeter initial mass function (IMF). This radius contains all of the baryonic material associated with the galaxy and is well outside the region compromised by numerical resolution effects. All of the rotation speeds are also computed at that radius. Note that $r_{\rm gal}$ exceeds the radii at which Tully-Fisher velocities are typically measured, but given the lower resolution of these simulations, rotation speeds at smaller radii are quite uncertain. This comparison therefore assumes that the circular velocity curves of actual disk galaxies remain approximately flat out to $r_{\rm gal}$.

4.2.2. *The I-Band Tully-Fisher Relation*

Figure 7 compares the observed I-band Tully-Fisher relation (*dots*) with the numerical results for galaxies selected in the fiducial $S_{0.9}$ ΛCDM model (*filled squares*) and in the W_1 WDM model (*filled triangles*). There is reasonable agreement between observation and simulations. The slope of the numerical TF relation is consistent with the observed value, and the scatter is much smaller (0.12 mag rms for $S_{0.9}$

[8] This error originated in the fact that NS00a used the transfer function proposed by Davis et al. (1985) to displace particles while normalizing the power spectrum using the value at the Nyquist frequency of the original low-resolution simulation given by the CDM transfer function fit of Bardeen et al. (1986). At this small scale, the two fits give power spectrum values that differ by almost a factor of 2, and this led to a systematic discrepancy between actual and intended normalizations. This error affected only the ΛCDM models of NS00a and NS00b. All other models, including NFW's, are free from this problem.

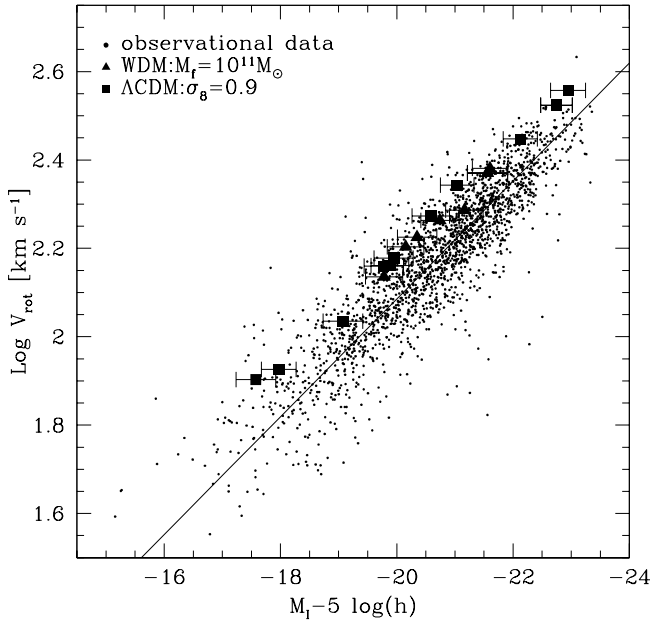

FIG. 7.—*I*-band Tully-Fisher relation compared to the result of numerical simulations in the fiducial $\sigma_8 = 0.9$ ΛCDM (*filled squares*) and in the W_1 warm dark matter (*filled triangles*) scenarios. Dots are a compilation of the data by Giovanelli et al. (1997), Mathewson, Ford, & Buchhorn (1992), and Han & Mould (1992). The solid line is the best fit to the data advocated by Giovanelli et al. Horizontal "error bars" in the simulation results span the range in luminosities derived from assuming a Scalo or a Salpeter IMF. Simulation circular velocities are measured at $r_{gal} = 20(V_{200}/220$ km s$^{-1}) h^{-1}$ kpc. Note that the slope, scatter, and zero point of the numerical TF relation are all in reasonable agreement with observation.

and 0.10 mag rms for W_1) than observed. These two conclusions are in agreement with the results of NS00a and NS00b.

The main difference with those works is that now even the zero point of the numerical relation appears to match reasonably well the observed value: the zero-point offset between simulations and observations is ~ 0.5 mag, compared with the 1.5 mag offset reported by NS00a and NS00b. The reason for the discrepancy can again be traced to the lower concentrations of $S_{0.9}$ halos compared with the results of NS00a and NS00b.[9] Figure 7 also shows that there is little difference in the TF results obtained for W_1 or $S_{0.9}$, supporting the interpretation that the halo concentration is the main factor responsible for the zero point of the numerical TF relation.

The 0.5 mag difference between simulation and observation is not too worrying given that the simulated galaxies have colors that are slightly too red compared with their TF counterparts. The average $B-R$ color of the simulated galaxies is 1.2, with little dependence on luminosity. For comparison, the average $B-R$ in Courteau's (1997) sample is ~ 0.8. This suggests that star formation in the simulations occurs too early. Any modification to the feedback algorithm that remedies this will also tend to increase the total luminosity in the simulated galaxies, because the younger stars are likely to emit sufficient extra radiation to overcome any decrease in the numbers of stars formed with stronger feedback. If this correction can bring the stellar *I*-band mass-to-light ratios down from 2.5 to 1.5, a value more in keeping with the results of Bell & de Jong (2001), then the 0.5 mag gap should be possible to bridge.

In summary, it appears that if the *I*-band stellar mass-to-light ratio of TF galaxies is of order $(M/L)_I \approx 1.5$, then ΛCDM halos are consistent with the slope, scatter, and zero point of the *I*-band Tully-Fisher relation. Note, however, that while halos formed in the fiducial ΛCDM scenario appear to have concentrations consistent with observational constraints, other problems associated with the assembly of disk galaxies through merging persist. In particular, the angular momentum (and size) of simulated disks is still quite below observed values, again suggesting that perhaps the feedback algorithm is not effective enough at preventing the early collapse of baryons into protogalactic potential wells (Navarro & Steinmetz 1997). Accounting simultaneously for the luminosity, velocity, and angular momentum of spiral galaxies in these models remains a challenging problem for the ΛCDM cosmogony.

5. SUMMARY AND CONCLUSIONS

This paper contains the results from an extensive suite of numerical simulations that were aimed at understanding the relationship between the power spectrum of initial density fluctuations and the concentration of virialized dark matter halos. These simulations demonstrate that dark halo concentration depends both on the amplitude of mass fluctuations as well as on the shape of the power spectrum. A simple model that takes this into account by defining an effective amplitude as $\sigma(M)$ times the logarithmic derivative of $\sigma(M)$ with respect to mass on scales similar to the characteristic mass of the halo (i.e., that enclosed within the radius where the circular velocity peaks, $r_{max} = 2.17 r_s$) has been developed. This model reproduces the mass and redshift dependence of the concentration in all seven cosmogonies investigated here, as well as in the eight different cosmogonies probed by NFW. It also extends the earlier models of NFW and Bullock et al. (2001) to power spectra very different from CDM, including truncated power spectra such as those appropriate for WDM.

These findings are applied to the Milky Way, where observational limits on the dark matter content within the solar circle can be turned into constraints on the shape and normalization of the power spectrum. For the popular ΛCDM spectrum, the Milky Way halo mass and the normalization of the power spectrum must satisfy the condition $\sigma_8 v_{220} m_{dark} < 0.8$, where v_{220} is the circular velocity of the halo (V_{200}) in units of 220 km s^{-1} and m_{dark} is the upper limit on the mass of dark matter within 8.5 kpc of the middle of the Milky Way in units of $4.3 \times 10^{10}\ M_\odot$. For $\sigma_8 = 0.9$, the normalization favored from the abundance of galaxy clusters and cosmic microwave background studies, this implies that the Milky Way halo has a circular velocity significantly smaller than the rotation speed at the solar circle, $V_{200} < 195$ km s^{-1}. This finding may have significant impact on the luminosity function expected in this model, since 195 km s^{-1} halos are much more abundant than their 220 km s^{-1} counterparts (see, e.g., Cole et al. 1994, 2000). Gasdynamical simulations including star formation and feedback also show that, because of their lower concentration relative to the NS00a and NS00b studies, ΛCDM halos are also roughly consistent with the zero point of the *I*-band

[9] The normalization problem only affected the ΛCDM runs in those papers. All the results concerning the standard $\Omega = 1$ CDM model remain unchanged.

Tully-Fisher relation. The slope and scatter of this relation are also in good agreement with observed values.

Halo concentrations in ΛCDM simulations are much lower than found by NS00a and NS00b, who argued that ΛCDM halos were too concentrated to be consistent with observations of the dynamics of spiral galaxies. A reanalysis of their data set reveals an inconsistency in the normalization of the power spectrum used in those works. Instead of the intended $\sigma_8 = 1.14$, their simulations had an effective normalization of $\sigma_8 \approx 1.6$. Once this correction is taken into account, their studies and our study yield consistent results.

The set of simulations reported here thus identify and illustrate the tight relation between power spectrum and halo concentrations. The application of these results to the Milky Way and *I*-band Tully-Fisher relation lifts previous concerns and suggests that the concentration of $\sigma_8 = 0.9$ ΛCDM halos is not clearly incompatible with observations.

We thank Carlos Frenk for helpful discussions. This work has been supported by the National Aeronautics and Space Administration under NASA grant NAG5-7151, by NSF grant 98-70151, and by NSERC research grant 203263-98. M. S. and J. F. N. are supported in part by fellowships from the Alfred P. Sloan Foundation. M. S. is also supported by a fellowship from the David and Lucile Packard Foundation. This research was supported in part by the National Science Foundation under grant PHY 94-07194.

REFERENCES

Avila-Reese, V., Colin, P., Valenzuela, O., D'Onghia, E., & Firmani, C. 2001, ApJ, submitted (astro-ph/0010525)
Bardeen, J. M., Bond, J. R., Kaiser, N., & Szalay, A. S. 1986, ApJ, 304, 15
Bell, E. F., & de Jong, R. S. 2001, ApJ, 550, 212
Bode, P., Ostriker, J. P., & Turok, N. 2000, BAAS, 197, 72.04
Bullock, J. S., Kolatt, T. S., Sigad, Y., Somerville, R. S., Kravtsov, A. V., Klypin, A. A., Primack, J. R., & Dekel, A. 2001, MNRAS, 321, 559
Carollo, C. M., de Zeeuw, P. T., van der Marel, R. P., Danziger, I. J., & Qian, E. E. 1995, ApJ, 441, L25
Cole, S., Aragon-Salamanca, A., Frenk, C. S., Navarro, J. F., & Zepf, S. E. 1994, MNRAS, 271, 781
Cole, S., Lacey, C., Baugh, C. M., & Frenk, C. S. 2000, MNRAS, 319, 168
Couchman, H. M. P. 1991, ApJ, 368, L23
Courteau, S. 1997, AJ, 114, 2402
Cretton, N., Rix, H.-W., & de Zeeuw, P. T. 2000, ApJ, 536, 319
Davis, M., Efstathiou, G., Frenk, C. S., & White, S. D. M. 1985, ApJ, 292, 371
Dehnen, W., & Binney, J. J. 1998, MNRAS, 294, 429
Dubinski, J., & Carlberg, R. 1991, ApJ, 378, 496
Eke, V. R., Cole, S., & Frenk, C. S. 1996, MNRAS, 282, 263
Eke, V. R., Navarro, J. F., & Frenk, C. S. 1998, ApJ, 503, 569
Flores, R. A., & Primack, J. R. 1994, ApJ, 427, L1
Flores, R. A., Primack, J. R., Blumenthal, G. R., & Faber, S. M. 1993, ApJ, 412, 443
Frenk, C. S., White, S. D. M., Davis, M., & Efstathiou, G. 1988, ApJ, 327, 507
Gerhard, O. 2000, in ASP Conf. Ser. 230, Galaxy Disks and Disk Galaxies, ed. J. G. Funes, S. J., & E. M. Corsini (San Francisco: ASP), in press (astro-ph/0010539)
Gerhard, O., Jeske, G., Saglia, R. P., & Bender, R. 1998, MNRAS, 295, 197
Giovanelli, R., Haynes, M. P., Herter, T., Vogt, N. P., Wegner, G., Salzer, J. J., da Costa, L. N., & Freudling, W. 1997, AJ, 113, 22
Han, M., & Mould, J. R. 1992, ApJ, 396, 453
Hogan, C. J., & Dalcanton, J. J. 2000, Phys. Rev. D, 62, 063511
Hu, W., Barkana, R., & Gruzinov, A. 2001, Phys. Rev. Lett., submitted (astro-ph/0003365)
Huss, A., Jain, B., & Steinmetz, M. 1999, MNRAS, 308, 1011
Klypin, A. A., Kravtsov, A. V., Bullock, J. S., & Primack, J. R. 2001, ApJ, submitted (astro-ph/0006343)
Klypin, A. A., Kravtsov, A. V., Valenzuela, O., & Prada, F. 1999, ApJ, 522, 82
Kravtsov, A. V., Klypin, A. A., Bullock, J. S., & Primack, J. R. 1998, ApJ, 502, 48
Kronawitter, A., Saglia, R. P., Gerhard, O., & Bender, R. 2000, A&AS, 144, 53
Lacey, C., & Cole, S. 1993, MNRAS, 262, 627
———. 1994, MNRAS, 271, 676
Liddle, A. R., Lyth, D. H., Viana, P. T. P., & White, M. 1996, MNRAS, 282, 281
Mathewson, D. S., Ford, V. L., & Buchhorn, M. 1992, ApJS, 81, 413
McGaugh, S. S., & de Blok, W. J. G. 1998, ApJ, 499, 41
Moore, B. 1994, Nature, 370, 629
Moore, B., Ghigna, S., Governato, F., Lake, G., Quinn, T., Stadel, J., & Tozzi, P. 1999a, ApJ, 524, L19
Moore, B., Governato, F., Quinn, T., Stadel, J., & Lake, G. 1998, ApJ, 499, L5
Moore, B., Quinn, T., Governato, F., Stadel, J., & Lake, G. 1999b, MNRAS, 310, 1147
Navarro, J. F., Frenk, C. S., & White, S. D. M. 1996, ApJ, 462, 563
———. 1997, ApJ, 490, 493
Navarro, J. F., & Steinmetz, M. 1997, ApJ, 478, 13
———. 2000a, ApJ, 528, 607 (NS00a)
———. 2000b, ApJ, 538, 477 (NS00b)
Navarro, J. F., & White, S. D. M. 1993, MNRAS, 265, 271
Peebles, P. J. E. 1980, The Large Scale Structure of the Universe (Princeton: Princeton Univ. Press)
———. 2000, ApJ, 534, L127
Press, W. H., & Schechter, P. 1974, ApJ, 187, 425
Rix, H.-W., de Zeeuw, P. T., Cretton, N., van der Marel, R. P., & Carollo, C. M. 1997, ApJ, 488, 702
Sommer-Larsen, J., & Dolgov, A. 2001, ApJ, 551, 608
Spergel, D. N., & Steinhardt, P. J. 2000, Phys. Rev. Lett., 84, 3760
Steinmetz, M. 1996, MNRAS, 278, 1005
Steinmetz, M., & Navarro, J. F. 1999, ApJ, 513, 555
Stompor, R., Gorski, K. M., & Banday, A. J. 1995, MNRAS, 277, 1225
Sugimoto, D., Chikada, Y., Makino, J., Ito, T., Ebisuzaki, T., & Umemura, M. 1990, Nature, 345, 33
Sugiyama, N. 1995, ApJS, 100, 281
Swaters, R. A. 1999, Ph.D. thesis, Rijksuniversiteit Groningen
Swaters, R. A., Madore, B. F., & Trewhella, M. 2000, ApJ, 531, L107
Tully, R. B., & Fisher, J. R. 1977, A&A, 54, 661
Tytler, D., O'Meara, J. M., Suzuki, N., & Lubin, D. 2000, Phys. Scr., 85, 12
van den Bosch, F. C., Robertson, B. E., Dalcanton, J. J., & de Blok, W. J. G. 2000, AJ, 119, 1579
van den Bosch, F. C., & Swaters, R. A. 2000, MNRAS, submitted (astro-ph/0006048)
Warren, M. S., Quinn, P. J., Salmon, J. K., & Zurek, W. H. 1992, ApJ, 399, 405